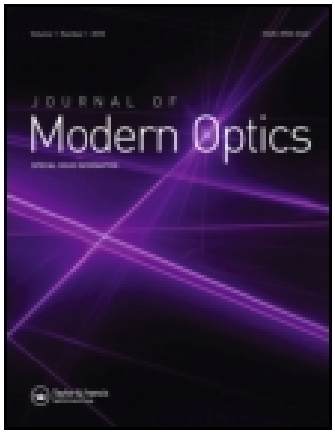

Journal of Modern Optics
Publication details, including instructions for authors and subscription information:
http://www.tandfonline.com/loi/tmop20

Controllable steep dispersion with gain in a four-level N-scheme with four-wave mixing

Nathaniel B. Phillips [a], Irina Novikova [a], Eugeniy E. Mikhailov [a], Dmitry Budker [b c] & Simon Rochester [b]

[a] Department of Physics, The College of William and Mary, Williamsburg, VA 23185, USA

[b] Rochester Scientific, LLC, El Cerrito, CA 94530, USA

[c] Department of Physics, University of California, Berkeley, CA 94720, USA

Published online: 26 Oct 2012.

To cite this article: Nathaniel B. Phillips, Irina Novikova, Eugeniy E. Mikhailov, Dmitry Budker & Simon Rochester (2013) Controllable steep dispersion with gain in a four-level N-scheme with four-wave mixing, Journal of Modern Optics, 60:1, 64-72, DOI: 10.1080/09500340.2012.733433

To link to this article: http://dx.doi.org/10.1080/09500340.2012.733433

Journal of Modern Optics, 2013
Vol. 60, No. 1, 64–72, http://dx.doi.org/10.1080/09500340.2012.733433

Taylor & Francis
Taylor & Francis Group

Controllable steep dispersion with gain in a four-level *N*-scheme with four-wave mixing

Nathaniel B. Phillips[a], Irina Novikova[a]*, Eugeniy E. Mikhailov[a], Dmitry Budker[b,c] and Simon Rochester[b]

[a]*Department of Physics, The College of William and Mary, Williamsburg, VA 23185, USA;* [b]*Rochester Scientific, LLC, El Cerrito, CA 94530, USA;* [c]*Department of Physics, University of California, Berkeley, CA 94720, USA*

(*Received 16 April 2012; final version received 15 September 2012*)

We present a theoretical analysis of the propagation of light pulses through a medium of four-level atoms, with two strong pump fields and a weak probe field in an *N*-scheme arrangement. We show that four-wave mixing has a profound effect on the probe-field group velocity and absorption, allowing the probe-field propagation to be tuned from superluminal to slow-light regimes with amplification.

Keywords: four-wave mixing; superluminal light; pulse propagation; optical gyroscope

1. Introduction

Precise rotation sensors are critical components for stabilization, navigation, and targeting applications. At the moment, the most sensitive commercial devices are optical gyroscopes based on the Sagnac effect [1]. Such a device consists of a ring interferometer with two counter-propagating light waves, as shown in Figure 1. The rotation of such an interferometer results in a phase difference between the two optical fields proportional to the magnitude of the rotational angular velocity $\vec{\Omega}$:

$$\Delta\phi = \frac{4\pi\omega}{c^2}\vec{A}\cdot\vec{\Omega}, \tag{1}$$

where ω is the light angular frequency, c is the speed of light, and $\vec{A}$ is the area of the optical loop. The most successful realizations to date are fiber-optics gyroscopes, in which the interferometer ring is formed by a loop of an optical fiber. The sensitivity of such an interferometer is usually boosted by using a large number N of loops that increase the effective area in Equation (1) by a factor of N. The Sagnac phase shift can be measured directly from the interference of the two counter-propagating waves at the output, or by monitoring the resulting frequency difference between corresponding counter-propagating modes of the interferometer cavity. In either case, the reciprocity of light propagation dramatically reduces effects of environmental factors (temperature, vibrations, etc.), and enhances reliability. As a result, the sensitivity of state-of-the-art compact fiber-optic gyroscopes has reached the shot-noise-limited value of 10^{-7}–10^{-8} rad s^{-1} $Hz^{-1/2}$ [2], while large-area laser gyroscopes have achieved even greater sensitivities, on the order of 10^{-10} rad s^{-1} $Hz^{-1/2}$ [3].

Similar sensitivity has been also achieved with matter-based Sagnac interferometers. In this case, the rotation-induced phase equation may be written as

$$\Delta\phi = \frac{4\pi}{\lambda_{\mathrm{dB}}v}\vec{A}\cdot\vec{\Omega}, \tag{2}$$

where v and $\lambda_{\mathrm{dB}} = 2\pi\hbar/(mv)$ represent the velocity and the de Broglie wavelength of the massive particles, respectively. Here, the advantage gained by the use of massive particles ($mc^2 \gg \hbar\omega$) is offset by the much smaller effective area compared to fiber-optics devices, resulting in similar performance [4].

Recent demonstrations of slow light pulse propagation in coherent optical media stirred active debate on the possibility of using slow-light pulses to enhance the Sagnac effect. It was quickly established that neither large positive ('slow light') nor negative ('fast light') dispersion has a *direct* influence on the magnitude of the Sagnac phase shift in Equation (1) [5].

Nevertheless, it still seems to be possible to take advantage of a large group index to enhance gyroscopic performance. For example, the output signal of a rotating interferometer with a highly dispersive slow-light medium can be enhanced by its differential response to opposite Sagnac phase shifts of two counter-propagating light waves [6]. A modest factor-of 2.5 enhancement of the observed phase difference has been recently demonstrated in a slow-light fiber ring [7], and a more significant enhancement (up to a factor of 200) is predicted in certain coupled resonator structures [6].

*Corresponding author. Email: inovikova@physics.wm.edu

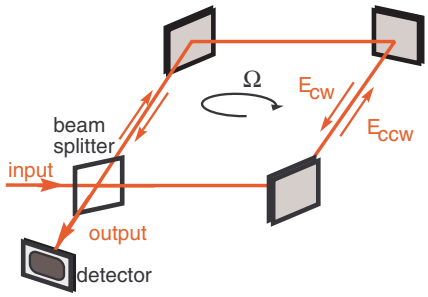

Figure 1. A generic schematic of an optical gyroscope based on the Sagnac effect. (The color version of this figure is included in the online version of the journal.)

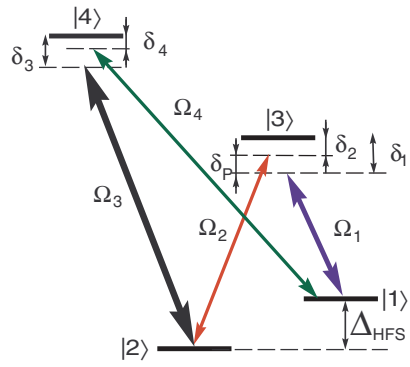

Figure 2. Schematic for three optical fields $\Omega_{1,2,3}$ interacting with four-level atoms in an N-configuration. A fourth field Ω_4, generated by four-wave mixing, may also be included, as described in the text. (The color version of this figure is included in the online version of the journal.)

Even more dramatic improvements are predicted for the measurement of the Sagnac-effect-induced mode splitting in an active ring cavity with strong negative dispersion [8]. Calculations have shown that the resulting frequency difference between two counter-propagating modes is inversely proportional to the group index, and thus nominally diverges for $n_g = 0$ (i.e. for $n \simeq -\omega(\partial n/\partial\omega)$) [8,9]. While this divergence disappears after correcting for higher-order nonlinear effects, a 10^6 improvement in gyroscope sensitivity should still be possible [8].

The current status of these debates shows that while strong positive or negative optical dispersion may indeed be capable of dramatic improvements in optical gyroscope performance, there is no clear winning approach. Thus, an atomic system that can be easily reconfigured to exhibit either strong positive or strong negative dispersion is an ideal candidate for the development of such a new generation of advanced optical gyroscopes. In the last decade, controllable manipulations of the group velocity of light have been demonstrated in a wide range of systems [10,11]. Nevertheless, atomic systems with long-lived spin coherences still provide the largest values of group index in both the slow and fast light regimes [12]. In such atomic systems, the group velocity for a probe optical field can be widely tuned by adjusting parameters of a strong control field that provides strong coupling of the probe optical field to a collective atomic spin state [13].

An ideal test system for the development of a new type of optical gyroscope with improved rotational sensitivity should have a dispersion that can be continuously controlled in the widest possible range – from the highest positive group index to the highest negative group index – with minimal changes in the experimental arrangement. While several interaction schemes are capable of such wide tunability [14,15], a so-called N-scheme has recently emerged as a promising candidate [16–20]. A possible realization of an N-scheme is via three optical fields interacting with four-level atoms in the arrangement shown in Figure 2 (omitting for now the field Ω_4). The strong control (Ω_1) and weak probe (Ω_2) fields by themselves form a regular Λ system exhibiting electromagnetically induced transparency (EIT) and slow light [13]. The interaction of the atoms with the second strong control field Ω_3 splits this single EIT peak into two, separated by a narrow enhanced-absorption peak. This spectral region exhibits a fast-light effect, desired for gyroscope performance enhancement. However, this fast-light regime cannot be directly utilized in the proposed active enhanced-sensitivity optical gyroscope due to its unavoidable high optical losses.

In this manuscript, we provide an extended treatment of the four-level N-scheme that includes the possibility of four-wave mixing (FWM) by allowing optical transitions (and spontaneous decay) between states $|4\rangle$ and $|1\rangle$. The associated FWM gain modifies the transmission of the probe field [21,22], and provides a smooth switch between slow- and fast-light regimes by varying the strength of one of the pump fields (Ω_3).

2. Slow and fast light in a four-level N-scheme

The evolution of a four-level N-system, shown in Figure 2, can be described under the rotating-wave approximation by the following Hamiltonian:

$$\hat{H} = \mathrm{i}\hbar \begin{pmatrix} 0 & 0 & -\frac{1}{2}\exp(-\mathrm{i}\phi_1)\Omega_1 & -\frac{1}{2}\exp(-\mathrm{i}\phi_4)\Omega_4 \\ 0 & -\delta_1+\delta_2 & -\frac{1}{2}\exp(-\mathrm{i}\phi_2)\Omega_2 & -\frac{1}{2}\exp(-\mathrm{i}\phi_3)\Omega_3 \\ -\frac{1}{2}\exp(\mathrm{i}\phi_1)\Omega_1 & -\frac{1}{2}\exp(\mathrm{i}\phi_2)\Omega_2 & -\delta_1 & 0 \\ -\frac{1}{2}\exp(\mathrm{i}\phi_4)\Omega_4 & -\frac{1}{2}\exp(\mathrm{i}\phi_3)\Omega_3 & 0 & -\delta_1+\delta_2-\delta_3 \end{pmatrix}, \quad (3)$$

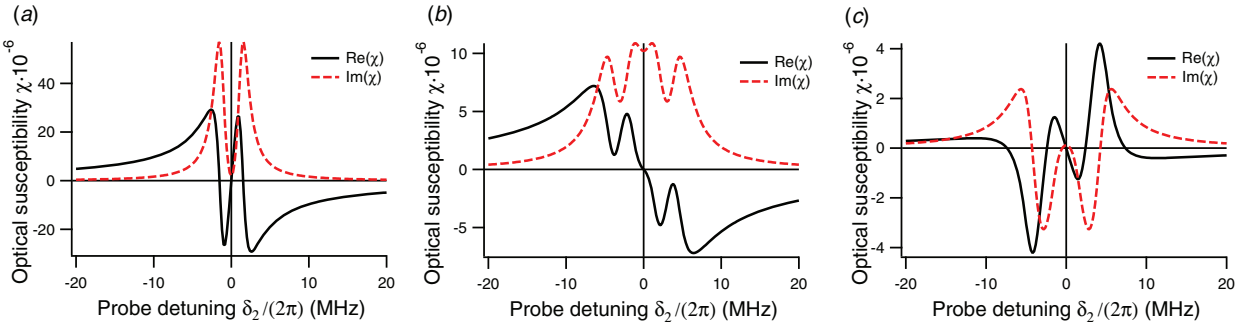

Figure 3. Real and imaginary parts of the probe-field susceptibility χ_P for various interaction configurations: (*a*) only one control field $\Omega_1 = (2\pi)\,3$ MHz is on (standard EIT regime); (*b*) both control fields $\Omega_1 = (2\pi)\,3$ MHz and $\Omega_3 = (2\pi)\,6$ MHz are present, but no radiative transition between states $|4\rangle$ and $|1\rangle$ is allowed (standard *N*-scheme); (*c*) both control fields $\Omega_1 = (2\pi)\,3$ MHz and $\Omega_3 = (2\pi)\,6$ MHz are present, and both excited states have equal decay rates into each of the ground states. For all graphs, the excited state decay rates are $\gamma_3 = \gamma_4 = (2\pi)\,3$ MHz, the ground-state relaxation rate is $(2\pi)\,0.01$ MHz, we assume equal branching ratios for all optical transitions, zero one-photon detunings for both pump fields, and atomic number density of 10^9 cm^{-3}. (The color version of this figure is included in the online version of the journal.)

where Ω_i and ϕ_i are the Rabi frequencies and phases of the corresponding optical fields, respectively, and δ_i are their detunings from the corresponding optical transitions, as shown in Figure 2. In this model we only considered interactions of each optical field with one atomic transition, as shown. Any far off-resonant couplings to other transitions will result, in first order, in additional light shifts of the corresponding levels; at high optical density they may considerably affect the pulse propagation dynamics, and must be included in calculation using, for example, Floquet analysis [23,24]. We also have assumed the four-photon resonance condition $-\delta_1 + \delta_2 - \delta_3 + \delta_4 = 0$, as well as the phase-matching condition on the optical wavenumbers k_i, $-k_1 + k_2 - k_3 + k_4 = 0$, which results in the elimination of the explicit time and space dependence from the Hamiltonian [25]. We note that the phase-matching condition is written in the scalar form because all wave vectors are collinear since the three applied fields are collinear. The four-photon resonance condition is automatically satisfied in the situation that we will primarily consider, in which the Stokes field Ω_4 is spontaneously generated. Namely, any variation in the probe two-photon detuning $\delta_P = \delta_2 - \delta_1$ is matched by the corresponding change in the Stokes field two-photon detuning $\delta_S = \delta_4 - \delta_3 = -\delta_P$.

The ability to control the dispersion of the probe field Ω_2 by adjusting the intensities of two strong control fields Ω_1 and Ω_3 is illustrated in Figure 3, obtained by numerically solving the evolution equations obtained from the above Hamiltonian for the steady-state condition. Figure 3(*a*) shows a traditional EIT regime, with a moderately strong first control field $\Omega_1 = (2\pi)\,3$ MHz and the second control field Ω_3 turned off. As expected, we observe a dip in the absorption spectrum (dashed line) and steep, positive, linear dispersion of the refractive index (solid line) near zero two-photon detuning $\delta_P = \delta_2 - \delta_1 = 0$, between two absorption peaks corresponding to the Autler–Townes splitting of the excited state by the strong control field. Figure 3(*b*) depicts the situation in which the atoms interact with both strong control fields Ω_1 and Ω_3 in a standard *N*-configuration, in which optical transition from state $|4\rangle$ to $|1\rangle$ is not allowed by selection rules. In this case, the spectrum consists of four partially-resolved absorption resonances, which can be interpreted as unequal Autler–Townes splittings of the states $|2\rangle$ and $|3\rangle$ by the control fields of different intensities $\Omega_1 = (2\pi)\,3$ MHz and $\Omega_3 = (2\pi)\,6$ MHz. Even though there are several spectral regions in which steep anomalous dispersion is realized, all of them occur in conjunction with enhanced absorption.

Finally, Figure 3(*c*) shows that the situation is quite different if optical transitions are allowed from both excited states to each of the ground states. In this case, the four-wave mixing process in a double-Λ system is possible, and it is enhanced through the long-lived spin coherence between states $|1\rangle$ and $|2\rangle$ [13,22,23]. As a result, a new optical Stokes field Ω_4 is efficiently generated (even though the input Stokes field is set to zero), and the probe-field transmission spectrum consists of two antisymmetric Raman resonances, with gain regions at both positive and negative probe-field detunings. For properly chosen intensities of the two control fields, it is possible to adjust the frequency splitting and widths of these peaks to achieve a negatively-sloped refractive index for the probe field near the zero two-photon detuning $\delta_P = 0$, while the gain drops to zero between the two gain peaks. Thus, the probe field experiences minimal absorption or gain

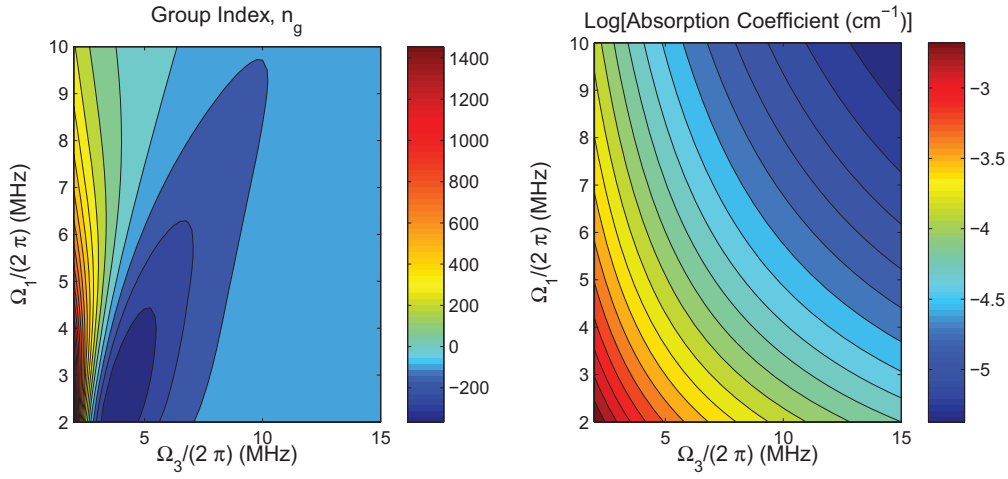

Figure 4. Probe-field group index $n_g \approx 1 + (\omega/2)\,\mathrm{Re}[\partial\chi_P/\partial\omega]$ (*left*) and the logarithm of the absorption coefficient $\log[(\omega/2c)\,\mathrm{Im}(\chi_P)]$, where the absorption coefficient is in cm^{-1} (*right*) as functions of both control fields' strengths. For this calculation, the experimental parameters are the same as in Figure 3. (The color version of this figure is included in the online version of the journal.)

for frequencies near the two-photon resonance, which are the desired characteristics of an atomic medium for gyroscope enhancement.

From this picture, it is clear that optimization of the control-field intensities allows for smooth tuning of the probe field's dispersion from slow to fast light regimes by changing the frequency shift and shape of the Raman peaks. To find the optimal operational parameters numerically, we computed the transmission spectrum for the probe field Ω_2 for the range of the control fields' Rabi frequencies and then calculate the dispersion, $\partial\chi_P/\partial\omega$, at the two-photon resonance. We display the on-resonance group index, $n_g \approx 1+(\omega/2)\,\mathrm{Re}[\partial\chi_P/\partial\omega]$, in the left-hand side graph in Figure 4. One can see that depending on the values of the intensities of the two control fields, the probe experiences either slow light (when the two gain peaks for positive and negative two-photon detuning are not resolved and form a single gain peak), or fast light (when the two peaks are farther apart, forming a distinct dip between them). In the graph, regimes exhibiting fast light are shown as dark blue, where as regimes exhibiting slow light behavior are indicated by the redder colors. When both fields are very strong, the Raman resonances are shifted too far from the origin, leading to flat dispersion. Additionally, we have investigated the absorption experienced by the probe field at the two-photon resonance, and we plot the resonant absorption coefficient, $(\omega/2c)\mathrm{Im}(\chi_P)$, in the right-most graph of Figure 4. We note that the units of the absorption coefficient are cm^{-1}. In this plot, the darker blue indicates less absorption than the dark red region, although in general, very little absorption is experienced for the selected ranges of Ω_1 and Ω_3. From this analysis we have identified $\Omega_1 = (2\pi)\,3\,\mathrm{MHz}$ and $\Omega_3 = (2\pi)\,6\,\mathrm{MHz}$ as suitable values for producing the desired fast-light behavior with vanishing absorption.

Under the four-wave mixing condition, the spontaneously generated Stokes field Ω_4 experiences strong gain, and thus its intensity increases as it propagates through the medium. Moreover, its presence has a strong effect on the probe field amplitude due to their mutual coupling through the atomic spin coherence, even though both probe and Stokes fields remain significantly weaker than either control field. In Figure 5, we plot the real and imaginary parts of optical polarizations for both the probe (top) and Stokes (bottom) fields, under conditions corresponding to different points along the optical path through the atomic medium. The left column represents the entrance of the vapor cell, where only the probe field is present, and $\Omega_4 = 0$ since it is not yet generated. Under these conditions, Ω_4 experiences strong gain, which leads to its spontaneous generation.

As the unattenuated probe light and generated Stokes field propagate along the cell, the increasing strength of Ω_4 starts affecting the propagation of the probe field through the FWM coupling. In particular, the negatively-sloped refractive index is somewhat flattened out, due to the appearance of a small amount of gain (Figure 5(*c*)). Farther along the cell, the probe field experiences stronger gain, but the dispersion switches to non-anomalous, associated with the slow-light propagation regime. The observed behavior indicates the amplitude of the Stokes field offers an additional control mechanism of the group

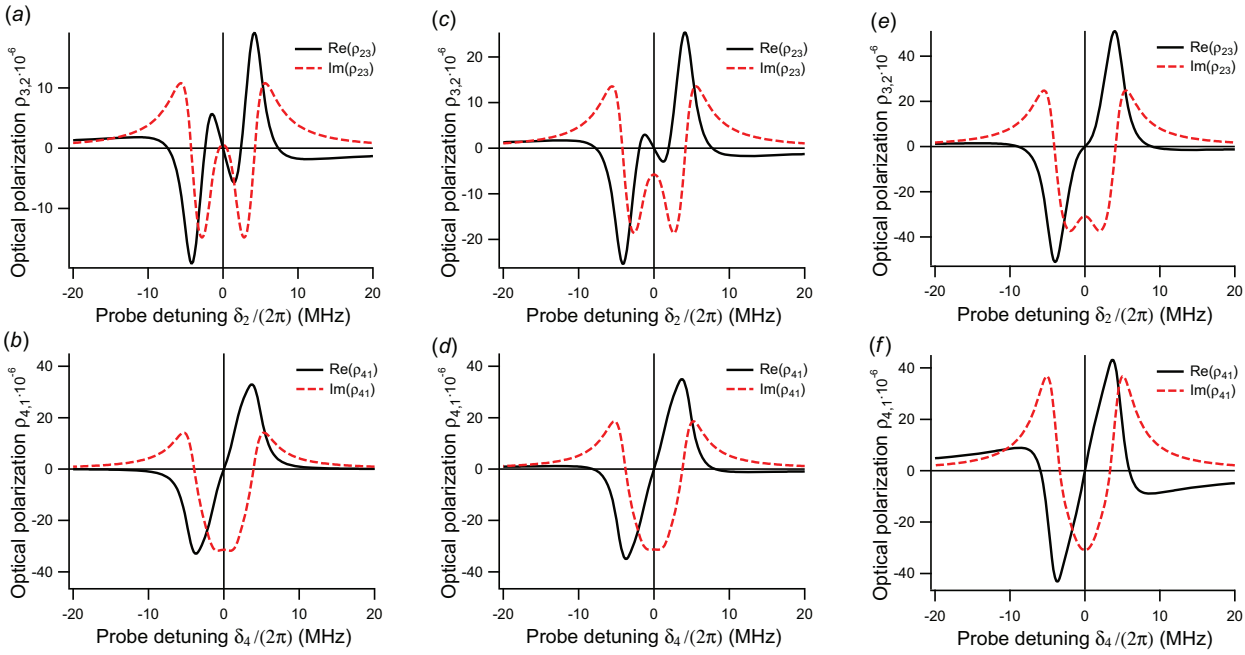

Figure 5. *Top row*: real and imaginary parts of atomic polarization $\rho_{3,2}$, proportional to the refractive index and absorption for the probe field Ω_2 for various strengths of the Stokes field. *Bottom row*: same for real and imaginary parts of atomic polarization $\rho_{4,1}$ for the Stokes field Ω_4. Pump fields are $\Omega_1 = (2\pi)\,3$ MHz and $\Omega_3 = (2\pi)\,6$ MHz, the probe field $\Omega_2 = (2\pi)\,1.0$ kHz; the values of the Stokes field are as follows: $\Omega_4 = 0$ for (*a*) and (*b*); $\Omega_4 = (2\pi)\,0.1\,\text{kHz} = \Omega_2/10$ for (*c*) and (*d*), and $\Omega_4 = (2\pi)\,1.0\,\text{kHz} = \Omega_2$ for (*e*) and (*f*). (The color version of this figure is included in the online version of the journal.)

index through, for example, the optical depth of the atomic ensemble. At the same time, the four-wave mixing process produces higher gain for the probe field at the output, and thus allows for compensation of unavoidable optical losses when operating inside a cavity.

3. Analytical solution

The results presented above were obtained by numerical solution of the propagation equations for all four optical fields using the interaction Hamiltonian of Equation (3) without making any additional assumptions about the parameters of the system. However, with a few reasonable approximations, we also can find an analytical solution for time-dependent weak optical fields Ω_2 and Ω_4 and strong cw optical fields Ω_1 and Ω_3. In this case we can assume a linear response of the atomic medium with respect to both weak optical fields. The strong control fields determine the populations of the atomic levels and optical polarizations for the $|1\rangle \rightarrow |3\rangle$ and $|2\rangle \rightarrow |4\rangle$ transitions that are coupled with these fields. Thus, the corresponding density matrix elements can be calculated assuming only the interaction of the two strong fields with the atoms, which in the interaction scheme under consideration (Figure 2) reduces to the simple case of two independent two-level systems, connected only through the decays of the excited states $|3\rangle$ and $|4\rangle$:

$$\dot{\rho}_{1,1} = \gamma_{31}\rho_{3,3} + \gamma_{41}\rho_{4,4} + \frac{1}{2}\mathrm{i}\Omega_1(\rho_{3,1} - \rho_{1,3}), \tag{4}$$

$$\dot{\rho}_{2,2} = \gamma_{32}\rho_{3,3} + \gamma_{42}\rho_{4,4} + \frac{1}{2}\mathrm{i}\Omega_2(\rho_{4,2} - \rho_{2,4}), \tag{5}$$

$$\dot{\rho}_{3,3} = -\gamma_3\rho_{3,3} - \frac{1}{2}\mathrm{i}\Omega_1(\rho_{3,1} - \rho_{1,3}), \tag{6}$$

$$\dot{\rho}_{4,4} = -\gamma_4\rho_{4,4} - \frac{1}{2}\mathrm{i}\Omega_2(\rho_{4,2} - \rho_{2,4}), \tag{7}$$

$$\dot{\rho}_{1,3} = -(\gamma_3/2 + \mathrm{i}\delta_1)\rho_{1,3} - \frac{1}{2}\mathrm{i}\Omega_1(\rho_{1,1} - \rho_{3,3}), \tag{8}$$

$$\dot{\rho}_{2,4} = -(\gamma_4/2 + \mathrm{i}\delta_3)\rho_{2,4} - \frac{1}{2}\mathrm{i}\Omega_3(\rho_{2,2} - \rho_{4,4}). \tag{9}$$

Here $\gamma_3 = \gamma_{31} + \gamma_{32}$ and $\gamma_4 = \gamma_{41} + \gamma_{42}$ are the population decay rates of the excited states. For simplicity, we have neglected the population decay rates from the two ground states, assuming that they are significantly smaller than the excited state decays and the strong optical fields' Rabi frequencies. Comparison with the

exact numerical solutions indicates that this is a good approximation.

Solving Equations (4)–(9) in the steady state and assuming equal branching ratios for the excited state decay channels ($\gamma_{31} = \gamma_{32} = \gamma_3/2$ and $\gamma_{41} = \gamma_{42} = \gamma_4/2$), we obtain the following expressions for the atomic populations and optical coherences:

$$\begin{pmatrix} \rho_{1,1}^{(0)} \\ \rho_{2,2}^{(0)} \\ \rho_{3,3}^{(0)} \\ \rho_{4,4}^{(0)} \\ \rho_{1,3}^{(0)} \\ \rho_{2,4}^{(0)} \end{pmatrix} = \frac{1}{T} \begin{pmatrix} \Omega_3^2(4\delta_1^2 + \Omega_1^2 + \gamma_3^2)\gamma_4 \\ \Omega_1^2(4\delta_3^2 + \Omega_3^2 + \gamma_4^2)\gamma_3 \\ \Omega_1^2\Omega_3^2\gamma_4 \\ \Omega_1^2\Omega_3^2\gamma_3 \\ -\Omega_1\Omega_3^2\gamma_4(2\delta_1 + \mathrm{i}\gamma_3) \\ -\Omega_3\Omega_1^2\gamma_3(2\delta_3 + \mathrm{i}\gamma_4) \end{pmatrix}, \tag{10}$$

where

$$T = 2{\Omega_3}^2\gamma_4\left(2{\delta_1}^2 + {\Omega_1}^2\right) + \gamma_3\gamma_4\left({\Omega_3}^2\gamma_3 + {\Omega_1}^2\gamma_4\right) + 2{\Omega_1}^2\gamma_3\left(2{\delta_3}^2 + {\Omega_3}^2\right)$$

is the common denominator. We make an additional approximation that the values of these density matrix elements do not change along the length of the cell. The validity of this approximation may be questioned, since, in fact, both strong fields will experience some absorption. Later we will demonstrate that, in the range of the strong-field intensities that produce the desired fast-light regime, this absorption is insignificant, and the non-depletion approximation is reasonable.

We are interested in calculating the propagation of the weak probe field Ω_2, as well as in the possible generation of the four-wave-mixing field Ω_4 connecting the $|4\rangle$ and $|1\rangle$ states, governed by the wave equations,

$$(-\mathrm{i}\omega + c\partial_z)\Omega_2 = \mathrm{i}g_2 N\rho_{3,2}, \tag{11}$$

$$(-\mathrm{i}\omega + c\partial_z)\Omega_4 = \mathrm{i}g_4 N\rho_{4,1}, \tag{12}$$

where $g_{2,4}$ are coupling coefficients for the corresponding optical transitions.

The remaining density matrix elements are described by the following equations:

$$\dot{\rho}_{1,2} = -\Gamma_{12}\rho_{1,2} + \frac{1}{2}\mathrm{i}\Omega_1\rho_{3,2} - \frac{1}{2}\mathrm{i}\Omega_3\rho_{1,4} - \frac{1}{2}\mathrm{i}\Omega_2\rho_{1,3}^{(0)} + \frac{1}{2}\mathrm{i}\Omega_4\rho_{4,2}^{(0)}; \tag{13}$$

$$\dot{\rho}_{1,4} = -\Gamma_{14}\rho_{1,4} + \frac{1}{2}\mathrm{i}\Omega_1\rho_{3,4} - \frac{1}{2}\mathrm{i}\Omega_3\rho_{1,2} + \frac{1}{2}\mathrm{i}\Omega_4(\rho_{4,4}^{(0)} - \rho_{1,1}^{(0)}); \tag{14}$$

$$\dot{\rho}_{3,2} = -\Gamma_{32}\rho_{3,2} + \frac{1}{2}\mathrm{i}\Omega_1\rho_{1,2} - \frac{1}{2}\mathrm{i}\Omega_3\rho_{3,4} - \frac{1}{2}\mathrm{i}\Omega_2(\rho_{3,3}^{(0)} - \rho_{2,2}^{(0)}); \tag{15}$$

$$\dot{\rho}_{3,4} = -\Gamma_{34}\rho_{3,4} + \frac{1}{2}\mathrm{i}\Omega_1\rho_{1,4} - \frac{1}{2}\mathrm{i}\Omega_3\rho_{3,2} + \frac{1}{2}\mathrm{i}\Omega_2\rho_{2,4}^{(0)} - \frac{1}{2}\mathrm{i}\Omega_4\rho_{3,1}^{(0)}; \tag{16}$$

where $\Gamma_{12} = \mathrm{i}(\delta_1 - \delta_2)$, $\Gamma_{14} = \gamma_4/2 + \mathrm{i}(\delta_1 - \delta_2 + \delta_3)$, $\Gamma_{32} = \gamma_3/2 - \mathrm{i}\delta_2$, and $\Gamma_{34} = (\gamma_3 + \gamma_4)/2 + \mathrm{i}(\delta_3 - \delta_2)$.

It is important to emphasize that we assume that the detuning of the generated field is such that it always obeys the four-photon resonance condition $-\delta_1 + \delta_2 - \delta_3 + \delta_4 = 0$. For example, if both strong fields are tuned to the atomic transition frequencies ($\delta_1 = \delta_3 = 0$) and the probe field detuning δ_2 is scanned, the detuning of the generated Stokes field changes in the opposite direction $\delta_4 = -\delta_2$ to maintain the resonance.

Equations (13)–(16) can be compactly written as

$$\dot{\rho}_{\downarrow} = M\rho_{\downarrow} + B, \tag{17}$$

where the vector $\rho_{\downarrow}$ consists of the four unknown density matrix elements $(\rho_{\downarrow})^{\mathrm{T}} = \{\rho_{1,2}, \rho_{1,4}, \rho_{3,2}, \rho_{3,4}\}$, M is a 4×4 matrix:

$$M = \begin{pmatrix} \mathrm{i}\delta_2 & -\mathrm{i}\Omega_3/2 & \mathrm{i}\Omega_1/2 & 0 \\ -\mathrm{i}\Omega_3/2 & \mathrm{i}\delta_2 - \gamma_4/2 & 0 & \mathrm{i}\Omega_1/2 \\ \mathrm{i}\Omega_1/2 & 0 & \mathrm{i}\delta_2 - \gamma_3/2 & -\mathrm{i}\Omega_3/2 \\ 0 & \mathrm{i}\Omega_1/2 & -\mathrm{i}\Omega_3/2 & \mathrm{i}\delta_2 - \gamma_3/2 - \gamma_4/2 \end{pmatrix}, \tag{18}$$

and B is defined as

$$B = \frac{1}{\mathrm{i}T} \begin{pmatrix} \Omega_1\Omega_3(\Omega_2\Omega_3 + \Omega_1\Omega_4)\gamma_3\gamma_4 \\ \mathrm{i}{\Omega_3}^2\Omega_4\left({\Omega_1}^2\gamma_3 - {\Omega_1}^2\gamma_4 - \gamma_3^2\gamma_4\right) \\ \mathrm{i}{\Omega_1}^2\Omega_2\left({\Omega_3}^2\gamma_4 - {\Omega_3}^2\gamma_3 - \gamma_3\gamma_4^2\right) \\ \Omega_1\Omega_3(\Omega_1\Omega_2 + \Omega_3\Omega_4)\gamma_3\gamma_4 \end{pmatrix}. \tag{19}$$

In this case the solution of Equation (17) in the frequency domain is

$$\rho_{\downarrow}^{(1)} = -(M + \mathrm{i}\omega\mathbf{I})^{-1}B, \tag{20}$$

where $\mathbf{I}$ is the identity matrix. Finally, the calculated expressions for the density matrix elements $\rho_{3,2}$ and $\rho_{4,1}$ in terms of the optical-field Rabi frequencies must be substituted into Equations (11) and (12) to obtain the propagation equations for the probe and Stokes field in a self-consistent form:

$$\partial_z\begin{pmatrix} \Omega_2 \\ \Omega_4 \end{pmatrix} = \frac{\mathrm{i}Ng}{c} M_2 \begin{pmatrix} \Omega_2 \\ \Omega_4 \end{pmatrix}, \tag{21}$$

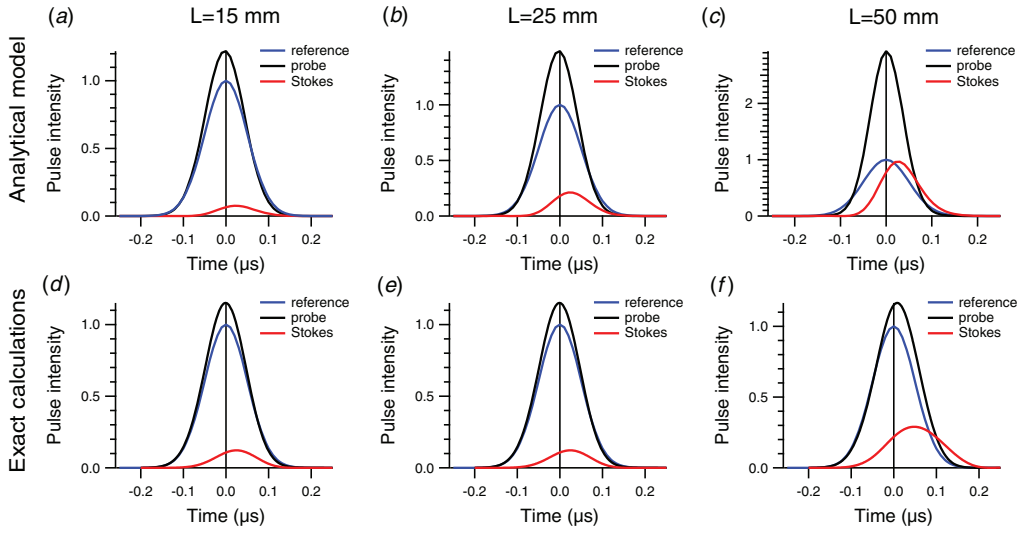

Figure 6. Comparison between exact solution (top) and approximate analytical calculations (bottom) of the signal pulse propagation through the cell of varying length. (The color version of this figure is included in the online version of the journal.)

where the matrix M_2 contains the information about atomic response, and we assume equal coupling coefficients $g_2 = g_4 = g$. The explicit form of the matrix M_2 consists of algebraic combinations of the Rabi frequencies and detunings of the strong optical fields and optical transition decay rates, but is omitted here for brevity.

The important consequence of the non-depletion approximation for the strong fields is that the right-hand side of Equation (21) does not depend on position z, allowing a direct solution:

$$\begin{pmatrix} \Omega_2(\omega,z) \\ \Omega_4(\omega,z) \end{pmatrix} = \exp\left(\frac{iNg}{c} M_2 z\right) \begin{pmatrix} \Omega_2(\omega,0) \\ \Omega_4(\omega,0) \end{pmatrix} \equiv \begin{pmatrix} A(\omega,z) & B(\omega,z) \\ C(\omega,z) & D(\omega,z) \end{pmatrix} \begin{pmatrix} \Omega_2(\omega,0) \\ \Omega_4(\omega,0) \end{pmatrix}. \quad (22)$$

Here $\Omega_{2,4}(0)$ are the Rabi frequencies corresponding to the input probe and Stokes fields. It is important to note that expanding the expressions for the coefficients A–D forms in a Taylor series up to the ω^2 terms accurately captures the pulse propagation dynamics, but allows significant speed-up in the calculations. The results presented below were obtained in this approximation.

Fourier transformation of the solution in Equation (22) to the time domain describes the propagation dynamics of the probe and Stokes optical fields. Figure 6 demonstrates the comparison between the exact numerical solutions obtained by calculating all time-dependent density matrix elements and propagation for all four optical fields (top graphs), and the prediction of our simplified analytical theory for propagation of a 100 ns Gaussian probe pulse through an atomic medium with density $10^9\,\mathrm{cm}^{-3}$ (bottom graphs). We observe that, for short lengths of the atomic medium (15 and 25 mm), the two methods provide similar solutions, predicting small gain and some advancement for the probe pulse, as well as generation of the Stokes pulse propagating with some delay. For the longer cell (50 mm), however, the analytical model significantly overestimates the gain in both probe and Stokes fields compared to the exact numerical solution that takes into account the attenuation of both strong control fields and the associated population redistribution. Nevertheless, it is interesting to note that both models predict positive delay for the probe pulse for the longer cell, with similar delay times.

The analytical solution also provides useful intuition about the role of the generated Stokes field in the dynamics of the probe optical field. For example, Figure 7 shows the real and imaginary parts of the coefficients A and B of the transfer matrix in Equation (22) for a relatively short atomic medium ($L = 1$ cm). The real part of these coefficients (Figure 7(a)) illustrates that both input probe and Stokes fields directly contribute to the predicted amplification of the probe field after the cell, and have no spectral dependence near the resonance. The imaginary parts of the coefficients, shown in Figure 7(b), represent the dispersive effect of the atomic medium. They are both nearly linear functions of frequency, with slopes of opposite sign. Also, for the chosen detunings, $\partial\mathrm{Im(B)}/\partial\omega$, representing the Stokes field contribution to the dispersion, is approximately twice as steep as $\partial\mathrm{Im(A)}/\partial\omega$. Thus, it is not surprising that for weak

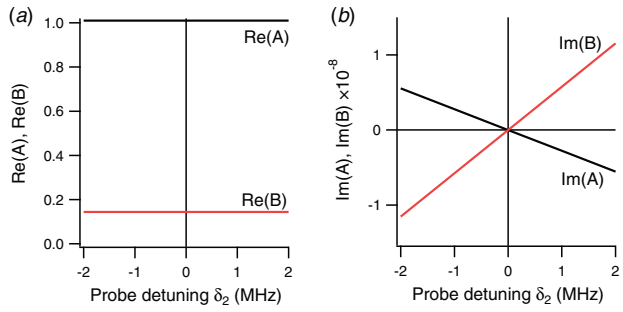

Figure 7. Coefficients A and B of the transfer matrix Equation (22) for near-zero probe detuning δ_2. The calculations are made for conditions identical to those of Figure 6(a). (The color version of this figure is included in the online version of the journal.)

Stokes fields (corresponding to low optical depth values), the dispersion is predominantly determined by the probe field propagation, and displays the 'fast light' regime. As the amplitude of the Stokes field increases, part of it is converted into the probe field via four-wave mixing. This additional contribution is associated with a positive dispersion, and eventually, overcomes the original negative dispersion of the probe field and changes its sign. Under these conditions, the output probe field is delayed, as in the 'slow light' regime.

4. Conclusions

In conclusion, we have analyzed the propagation of a weak resonant probe through a medium of four-level atoms in an N-scheme with allowed four-wave mixing generation, and found it to be a promising candidate for the realization of tunable 'slow-to-fast' light with no absorption. This is particularly interesting for the experimental investigation of potential techniques for the enhancement of optical-gyroscope performance, as well as for the development of white-light-cavity applications [26] for gravitational wave detection [27]. In addition, these results will contribute to a better understanding of the role of four-wave mixing in realization of single-photon nonlinear interactions in the N-scheme [28,29].

Acknowledgements

The authors thank Frank Narducci and John Davis for useful discussions. This research was supported by Naval Air Warfare Center STTR program N68335-11-C-0428.

References

[1] Sagnac, G. *C. R. Acad. Sci.* **1913,** *95,* 708–710.
[2] Lefevre, H.C. Application of the Sagnac Effect in the Interferometric Fiber-optic Gyroscope. In *Optical Gyros and Their Application*: Loukianov, D., Rodloff, R., Sorg, H., Stieler, B., Eds.; NATO: Neuilly-sur-Seine, France, 1999; RTO AGARDograph RTO-AG-339, pp 7:1–7:29.
[3] Stedman, G.E.; Schreiber, K.U.; Bilger, H.R. *Class. Quantum Gravity* **2003,** *20,* 2527.
[4] Gustavson, T.L.; Landragin, A.; Kasevich, M.A. *Class. Quantum Gravity* **2000,** *17,* 2385.
[5] Malykin, G.B. *Phys.-Usp.* **2000,** *43,* 1229.
[6] Peng, C.; Li, Z.; Xu, A. *Opt. Express* **2007,** *15,* 3864–3875.
[7] Zhang, Y.; Tian, H.; Zhang, X.; Wang, N.; Zhang, J.; Wu, H.; Yuan, P. *Opt. Lett.* **2010,** *35,* 691–693.
[8] Shahriar, M.S.; Pati, G.S.; Tripathi, R.; Gopal, V.; Messall, M.; Salit, K. *Phys. Rev. A* **2007,** *75,* 053807.
[9] Pati, G.S.; Salit, M.; Salit, K.; Shahriar, M.S. *Opt. Commun.* **2008,** *281,* 4931–4935.
[10] Boyd, R.W.; Gauthier, D.J.; Wolf, E. *Prog. Opt.* **2002,** *43,* 497–530, doi: 10.1016/S0079-6638(02)80030-0.
[11] Boyd, R.W.; Gauthier, D.J. *Science* **2009,** *326,* 1074–1077.
[12] Akulshin, A.M.; McLean, R.J. *J. Opt.* **2010,** *12,* 104001.
[13] Lukin, M.D. Colloquium: *Rev. Mod. Phys.* **2003**, *75*(2), 457.
[14] Akulshin, A.M.; Cimmino, A.; Sidorov, A.I.; Hannaford, P.; Opat, G.I. *Phys. Rev. A* **2003,** *67,* 011801.
[15] Mikhailov, E.E.; Sautenkov, V.A.; Novikova, I.; Welch, G.R. *Phys. Rev. A* **2004,** *69,* 063808.
[16] Harris, S.E.; Yamamoto, Y. *Phys. Rev. Lett.* **1998,** *81,* 3611.
[17] Kang, H.; Hernandez, G.; Zhu, Y. *Phys. Rev. A* **2004,** *70,* 011801.
[18] Yi, C.; Wei, X.G.; Ham, B.S. *J. Phys. B* **2009,** *42,* 065506.
[19] Abi-Salloum, T.Y.; Snell, S.; Davis, J.P.; Narducci, F.A. *J. Mod. Opt.* **2011,** *58,* 2008–2014.
[20] Abi-Salloum, T.Y.; Henry, B.; Davis, J.P.; Narducci, F. *Phys. Rev. A* **2010,** *82,* 013834.

[21] Fleischhaker, R.; Evers, J. *Phys. Rev. A* **2008,** *78,* 051802.
[22] Glasser, R.T.; Vogl, U.; Lett, P.D., *Phys. Rev. Lett.* **2012**, *108*, 173902.
[23] Phillips, N.B.; Gorshkov, A.V.; Novikova, I. *J. Mod. Opt.* **2009,** *56,* 1916–1925.
[24] Phillips, N.B.; Gorshkov, A.V.; Novikova, I. *Phys. Rev. A* **2011,** *83,* 063823.
[25] Mahmoudi, M.; Evers, J. *Phys. Rev. A* **2006,** *74,* 063827.
[26] Fleischhaker, R.; Evers, J. *Phys. Rev. A* **2008,** *78,* 051802.
[27] Salit, M.; Shahriar, M.S. *J. Opt.* **2010,** *12,* 104014.
[28] Braje, D.A.; Balić, V.; Yin, G.Y.; Harris, S.E. *Phys. Rev. A* **2003,** *68,* 041801.
[29] Bajcsy, M.; Hofferberth, S.; Balic, V.; Peyronel, T.; Hafezi, M.; Zibrov, A.S.; Vuletic, V.; Lukin, M.D. *Phys. Rev. Lett.* **2009,** *102,* 203902.